Published in final edited form as:
Proteins. 2010 August 1; 78(10): 2265–2282. doi:10.1002/prot.22739.

Allosteric Effects of the Anti-Psychotic Drug Trifluoperazine on the Energetics of Calcium Binding by Calmodulin

Michael D. Feldkamp[1], **Susan E. O'Donnell**[1], **Liping Yu**[2], and **Madeline A. Shea**[1,*]

[1]Department of Biochemistry Roy J. and Lucille A. Carver College of Medicine University of Iowa Iowa City, Iowa 52242-1109, USA

[2]NMR Facility Roy J. and Lucille A. Carver College of Medicine University of Iowa Iowa City, Iowa 52242-1109, USA

Abstract

Trifluoperazine (TFP; Stelazine™) is an antagonist of calmodulin (CaM), an essential regulator of calcium-dependent signal transduction. Reports differ regarding whether, or where, TFP binds to apo CaM. Three crystallographic structures (1CTR, 1A29, 1LIN) show TFP bound to $(Ca^{2+})_4$-CaM in ratios of 1, 2 or 4 TFP per CaM. In all of these, CaM domains adopt the "open" conformation seen in CaM-kinase complexes having increased calcium affinity. Most reports suggest TFP also increases calcium affinity of CaM. To compare TFP binding to apo CaM and $(Ca^{2+})_4$-CaM, and explore differential effects on the N- and C-domains of CaM, stoichiometric TFP titrations of CaM were monitored by ^{15}N-HSQC NMR. Two TFP bound to apo CaM, while four bound to $(Ca^{2+})_4$-CaM. In both cases, the preferred site was in the C-domain. During the titrations, biphasic responses for some resonances suggested inter-site interactions. TFP-binding sites in apo CaM appeared distinct from those in $(Ca^{2+})_4$-CaM. In equilibrium calcium titrations at defined ratios of TFP:CaM, TFP reduced calcium affinity at most levels tested; this is similar to the effect of many IQ-motifs on CaM. However, at the highest level tested, TFP raised the calcium affinity of the N-domain of CaM. A model of conformational switching is proposed to explain how TFP can exert opposing allosteric effects on calcium affinity by binding to different sites in the "closed", "semi-open" and "open" domains of CaM. In physiological processes, apo CaM, as well as $(Ca^{2+})_4$-CaM, needs to be considered a potential target of drug action.

Keywords

Allostery; ^{15}N-HSQC; NMR; Titration; Binding; Linkage

Introduction

Calmodulin (CaM) is a small (148 a.a.), essential, and highly conserved eukaryotic protein that is required for many calcium-sensitive signal transduction pathways [1,2]. It is composed of two homologous domains (N and C). Each domain consists of a pair of EF-hands (a helix-loop-helix motif) that forms a 4-helix bundle, and binds two calcium ions cooperatively. The domains are connected by a linker that plays a regulatory role in determining calcium affinity, and permits the domains to adopt multiple relative orientations to optimize interactions with target proteins (Fig. 1a) [3-5].

* To whom correspondence should be addressed. Telephone: (319) 335-7885. Fax: (319) 335-9570. madeline-shea@uiowa.edu.
PI of laboratory in which research was conducted: Prof. Madeline A. Shea, Ph.D.

Although the two domains are similar in sequence and structure, the affinity of the N-domain for calcium is an order of magnitude lower than that of the C-domain [6,7]. As the concentration of intracellular calcium increases, calcium binding to 12-residue sites in CaM triggers conformational changes, causing the pairs of helices in each 4-helix bundle to separate. This structural change associated with the transition from apo (calcium-depleted) to $(Ca^{2+})_4$-CaM exposes hydrophobic residues that alter the affinity of CaM for target proteins [8-11]. $(Ca^{2+})_4$-CaM (4 bound calcium ions) is shown in Fig. 1a.

In a CaM-target complex, the protein-protein interface is determined by the number and location of occupied calcium-binding sites of CaM, conformational change propagated from those binding sites, and the surface of the target protein. Based on the interhelical angles adopted by the paired helices of each domain, the CaM C-domain has been categorized as adopting three distinct conformations: “closed”, “semi-open”, and “open” [8-11]. Any of these may be adopted by free CaM (Fig. 1b), consistent with the hypothesis that changes in the distribution of pre-existing conformational states occur upon binding to Ca^{2+} or a target protein [12]. In high-resolution structures, only apo CaM has been observed to adopt the “closed” and “semi-open” forms, while only $(Ca^{2+})_4$-CaM has been observed in the “open” form (Fig. 1b). Binding of a target protein stabilizes the “semi-open” or “open” conformation of CaM by burying hydrophobic surface area that would otherwise be exposed to solvent. For example, a CaMKII peptide bound to calcium-saturated “open” CaM (1CM1.pdb) buries 1226 $Å^2$ of the surface area of CaM; of that, 990 $Å^2$ (81%) is hydrophobic [13].

For many years, activation of CaM-regulated target proteins such as metabolic enzymes, kinases, and phosphatases was thought to occur in a strictly calcium-dependent manner, such that the extent of binding of a target protein to apo CaM was negligible, and binding to $(Ca^{2+})_4$-CaM always increased its calcium affinity [14]. However, there are subclasses of CaM-regulated target proteins, including some ion channels, that contain IQ-motifs that reduce the calcium affinity of CaM [15,16]. These targets interact preferentially with apo CaM. The only high resolution structure of apo CaM interacting with an IQ-motif (2IX7.pdb) is the crystallographic observation of two apo CaM molecules bound to a peptide containing two adjacent IQ-motifs derived from Myosin V [17] (Fig. 1b). In this complex, both N-domains were “closed” whereas the C-domains were “semi-open”. Analysis of the CaM-peptide interface showed that hydrophobic residues of CaM accounted for most (71% and 75%) of the buried surface of the two CaM C-domains.

Drugs with aromatic moieties bind to CaM in a manner similar to protein targets that bury a phenylalanine or tryptophan residue in the hydrophobic pockets of CaM [18-20]. Trifluoperazine (TFP) (Fig. 1a) is a CaM antagonist historically used in the treatment of mental illness because of its interaction with the dopamine receptor; recently, it was implicated in the disruption of opioid tolerance [21]. TFP is membrane-permeable and is commonly added to cell culture media to disrupt CaM-mediated processes [22-24]. Structures of three TFP-CaM complexes [18-20] have been determined crystallographically. In these, 1, 2, or 4 molecules of TFP are bound to $(Ca^{2+})_4$-CaM; all of them share a TFP-binding site in the C-domain but only one structure (1LIN.pdb) has a TFP-binding site in the N-domain. Superposition of these structures showed that the backbone of CaM adopts indistinguishable conformations in all of them, despite differences in the number and location of TFP molecules bound (Fig. 1c). The relative abundance of these three ligation states of TFP bound to CaM in solution is not known. In all three complexes, the tertiary structure of CaM mimics that of $(Ca^{2+})_4$-CaM when bound to CaMKII, and other kinases that increase its calcium affinity [25-27].

The conflicting structural evidence regarding a preferred binding stoichiometry for TFP binding to CaM, as well as disagreement on the effects of TFP on the calcium-binding properties of CaM [18-20,28-30], motivated this study of the thermodynamic and structural properties of intermediate ligation states. These are critical for understanding how the highly homologous N- and C-domains of CaM exert different physiological effects on target proteins, and exploring whether exogenous, pharmaceutical applications of TFP and related drugs truly target only the calcium-saturated form of CaM, as has been assumed.

TFP titrations of CaM monitored by ^{15}N-HSQC spectroscopy showed that TFP saturated apo CaM at a ratio of 2:1, but saturated $(Ca^{2+})_4$-CaM at a ratio of 4:1. Equilibrium calcium titrations monitored by steady-state fluorescence spectroscopy demonstrated that, unlike the majority of effectors (e.g., peptides and proteins) whose binding to CaM has been examined in detail, TFP reduced the calcium affinity of CaM at low stoichiometries. Thus, thermodynamic linkage requires that TFP have a higher affinity for apo CaM than for $(Ca^{2+})_4$-CaM; this is similar to the preferential binding of most IQ-motifs to apo CaM.

However, the multiplicity of binding stoichiometries allows for reversal of this effect. At higher ratios (8:1) of TFP:CaM, the calcium affinity of CaM reversed, and was more favorable than that in the absence of TFP. These effects were found to be similar, but not identical, in each domain (N and C) of CaM and were compared to the effects of TFP on isolated domain fragments. On this basis, a model is proposed in which the “semi-open” conformation offers a “pocket” for binding of aromatic moieties that is unlike the FLMM pocket [31] of the “open” conformation where aromatic side chains of many peptides are known to bind to CaM. TFP recognizes this site on the “semi-open” conformation of an apo domain that is not available when CaM adopts the “open” conformation.

The binding preference of a single TFP molecule for apo CaM is significant because, to the best of our knowledge, it is the only drug identified to reduce calcium affinity. This motivates a review of studies in which TFP antagonizes CaM-dependent cellular phenomena. The interference observed in those studies has been interpreted as arising from the effects of the drug on $(Ca^{2+})_4$-CaM and its regulation of enzymes or channels. However, the findings presented here show that TFP can act as an antagonist of apo CaM, which is critical for regulating pathways that are distinct from those modulated by $(Ca^{2+})_4$-CaM.

Materials and Methods

Protein over-expression and purification

IPTG-induced over-expression of CaM was performed using transformed BL21 DE3 or BL21 DE3-pLysS cells containing the recombinant pT7-7 vector of interest: full-length mammalian CaM_{1-148}, CaM_{1-80}, and CaM_{76-148} [32]. For ^{15}N-labeled proteins used in the NMR studies, *Paramecium* CaM_{1-148} (PCaM) was over-expressed in minimal medium with ^{15}N-NH_4Cl (Cambridge Isotopes) as the sole nitrogen source. The proteins were then purified as described by Putkey [33]. The recombinant proteins were 97-99% pure as judged by silver-stained SDS-PAGE and reversed-phase HPLC. Protein concentrations were calculated from UV absorbance in 0.1 N NaOH, using the extinction coefficients for Phe and Tyr reported by Beaven and Holiday [34]

Equilibrium calcium titrations monitored by intrinsic protein fluorescence

Calcium titrations were monitored at 22 °C with a PTI-QM4 Fluorimeter (Proton Technology International, Birmingham, NJ) using bandpasses of 4 nm (for excitation) and 6 nm (for emission). CaM (CaM_{1-148}, CaM_{1-80}, or CaM_{76-148} at 6 μM) solutions, containing 0, 6, 12, 18, 24, or 48 μM TFP (Sigma-Aldrich, St. Louis, MO), were prepared in 50 mM HEPES, 100 mM KCl, 5 mM NTA, 0.05 mM EGTA, 1 mM $MgCl_2$, and 5.75 nM Oregon

Green (pH 7.4). The concentration of TFP was determined using an $\varepsilon_{305.5}$ of 3540 M^{-1} cm^{-1} [35]. CaM was titrated using a microburet (Micro-Metric Instrument Co., Cleveland, OH) fitted with a 250 μL Hamilton syringe (Hamilton Co., Reno, NV) containing a concentrated $CaCl_2$ solution prepared in a matching buffer. Binding of calcium to sites I and II in the N-domain was monitored with λ_{ex} of 250 nm, and λ_{em} of 280 nm, based on the intrinsic phenylalanine fluorescence. Binding to sites III and IV in the C-domain was monitored with λ_{ex} of 277 nm, and λ_{em} of 320 nm, based on the intrinsic tyrosine fluorescence as previously described [7]. The fluorescent calcium indicator dye Oregon Green 488 BAPTA-5N (Oregon Green, 5.75 nM) (Molecular Probes, Eugene, OR) was used to determine the free calcium concentration at each point in the titration according to Eq. 1,

$$[calcium]_{free} = K_d \frac{f_{[x]} - f_{low}}{f_{high} - f_{[x]}} \quad (1)$$

where f_{high} and f_{low} are the highest and lowest observed fluorescence intensity signals, respectively, observed for Oregon Green during the titration. The K_d of calcium binding to Oregon Green was determined previously to be 34.24 μM in 50 mM HEPES, 100 mM KCl, and 1 mM $MgCl_2$ (pH 7.4) at 22 C (λ_{ex} of 494 nm, λ_{em} of 521 nm) [7]. Each titration was repeated at least three times.

Free energies of calcium binding to the pair of sites in each domain were determined by fitting the titrations to a model-independent two-site (Adair) function (Eq 2), as described previously [7].

$$\bar{Y} = \frac{K_1 [X] + 2K_2 [X]^2}{2\left(1 + K_1 [X] + K_2 [X]^2\right)} \quad (2)$$

where [*X*] is free calcium, and the macroscopic association constant K_1 is the sum of intrinsic microscopic equilibrium constants ($k_1 + k_2$) for two sites: either sites I and II in the N-domain, or sites III and IV in the C-domain. This formulation allows the microscopic binding constants (k_1 and k_2) to be nonequivalent. The second macroscopic equilibrium constant K_2 ($k_1 k_2 k_c$) is the product of the intrinsic microscopic equilibrium constants (k_1, k_2) and the cooperativity constant (k_c). The parameters ΔG_1 and ΔG_2 are macroscopic binding free energies, with $\Delta G_i = -RT \ln K_i$. The parameter ΔG_2 is thus the total free energy of saturating both calcium-binding sites in a domain.

Changes in fluorescence intensity for the calcium titrations were normalized to the highest and lowest experimentally determined signals. To account for experimental variations in the asymptotes of replicate titrations, we performed nonlinear least-squares analysis of the fluorescence intensity signal using the function [*f(X)*], as given by Eq. 3

$$f(X) = Y_{[X]low} + \bar{Y} \bullet Span \quad (3)$$

where $\bar{Y}$ refers to the average fractional saturation as described by Eq. 2, and $Y_{[X]low}$ corresponds to the value of the fluorescence intensity in the absence of calcium. The parameter *Span* was negative in the case of a decreasing signal and positive in the case of an increasing signal. For monotonic titrations with well defined asymptotes, values for all parameters (ΔG_1, ΔG_2, $Y_{[X]low}$ and *Span*) were fit simultaneously using NONLIN [36,37].

Note that a ratio of N:1 TFP:CaM does not indicate that all CaM molecules in the solution have N TFP molecules bound. Dissociation constants (K_d) in the low μM range (1-5 μM) have previously been reported for TFP release from $(Ca^{2+})_4$-CaM; although, site-specific TFP binding affinities have not been reported [28,38]. The range of concentrations of TFP used in this study (6-48 μM) are well above the reported K_d values, insuring a significant population of TFP bound $(Ca^{2+})_4$-CaM at the ratios examined. It was not possible to determine the population distribution of TFP:CaM species in solution from an independent, experimentally observable property, the values of ΔG_2 determined in the presence of TFP are apparent values (i.e., ΔG_2^{app}).

NONLIN provides several measures of the goodness-of-fit for the parameters that minimize the variance of each fit. These error statistics include (a) the value of the square root of variance, (b) the values of asymmetric 65% confidence intervals, (c) the systematic trends in the distribution of residuals, (d) the magnitude of the span of residuals, and (e) the absolute value of elements of the correlation matrix. From these, best-fit values were selected after testing multiple sets of initial guesses for parameters to probe for the presence of local minima. Free energies determined from at least three replicate titrations were averaged; those values and standard deviations are reported in Table 1.

In some titrations, the value determined for ΔG_1 was sensitive to starting guesses; in those cases, a manual grid search was conducted to obtain the lowest square root of variance. For titrations (Fig. 6b, righthand insert) that exhibited alternating increasing and decreasing calcium-dependent changes in fluorescence intensity, it was necessary to fix the values of both ΔG_1, and Span, as described in the *Results* section. Estimates of the apparent total free energy corresponding to each transition are reported separately in Table 1.

NMR Spectra

^{15}N-HSQC spectra were acquired at 25 °C on a Bruker Avance II 800 MHz US^2 spectrometer with a 5 mm TXI ^{1}H (^{15}N/^{13}C/D) probe featuring XYZ gradients. All spectra were processed in NMRPipe/NMRDraw [39], while peak-picking and analysis were performed using SPARKY[40]. TFP titrations of ^{15}N-PCaM$_{1\text{-}148}$ under apo conditions were carried out in 10% D_2O, 10 mM imidazole, 100 mM KCl, 50 μM EDTA, pH 6.5 at 22°C; in the case of $(Ca^{2+})_4$-PCaM$_{1\text{-}148}$ TFP titration studies, 10 mM $CaCl_2$ was included. Starting volumes were 500 μL.

TFP titration of CaM Monitored by NMR

^{15}N-HSQC spectra of apo ^{15}N-PCaM$_{1\text{-}148}$ were acquired at incrementally increasing concentrations of TFP. The initial concentration of both apo- and $(Ca^{2+})_4$-^{15}N-PCaM$_{1\text{-}148}$ was 617 μM. In the TFP titration series performed under apo conditions, the $[TFP]_{total}$ was 0, 0.15, 0.29, 0.44, 0.61, 0.75, 0.90, 1.04, 1.21, 1.35, 1.49, 1.63, 1.79, 1.93, 2.07, and 2.37 mM (16 spectra). In the $(Ca^{2+})_4$-^{15}N-PCaM$_{1\text{-}148}$ TFP titration series, the $[TFP]_{total}$ was 0, 0.14, 0.28, 0.41, 0.58, 0.71, 0.85, 0.99, 1.15, 1.28, 1.41, 1.55, 1.70, 1.83, 1.96, 2.25, and 2.75 mM (17 spectra). The amide assignments for apo and $(Ca^{2+})_4$-^{15}N-PCaM$_{1\text{-}148}$ in the absence of TFP were reported previously [41]. To determine the change in chemical shift upon TFP binding to apo and $(Ca^{2+})_4$-PCaM$_{1\text{-}148}$, chemical-shift changes in both the ^{1}H and ^{15}N dimensions were quantified using the modified Pythagorean theorem shown in Eq. 4.

$$\Delta ppm = \left[\left(\Delta^1 H \,(800.224 \quad \text{Hz/ppm}) \right)^2 + \Delta^{15} N \,(81.095 \quad \text{Hz/ppm}) \right)^2 \Big]^{1/2} \tag{4}$$

In this equation, Δ*ppm* refers to the linear change of a specific resonance peak from its initial starting position as TFP is titrated into solution, as done previously [41].

Computational Modeling of TFP Binding

AutoDock Vina 1.0.3 [42] was used to simulate the binding of a single molecule of TFP to a fragment of CaM corresponding to the apo C-domain in three different tertiary conformations: “closed”, “semi-open” and “open”. Coordinates for residues 82-146 were extracted from these structures: 1DMO.pdb (apo, “closed”), 2IX7.pdb (apo, “semi-open”), 2HQW.pdb (calcium-saturated, “open”, bound to NR1C1 peptide), and 1LIN.pdb (calcium-saturated, “open”, 4 TFP molecules bound). To approximate an apo “open” structure (which has not been observed experimentally), calcium ions were removed from 2HQW and 1LIN. Each of the four protein fragments were placed in a cubic (45 $Å^3$) search space with implicit water. The exhaustiveness parameter was 128. In Fig. 8a, the 20 models that had the most favorable (lowest) free energies are depicted by PyMol™ v.1.2r2 (DeLano Scientific), using a gradient of green (most favorable) to white (least favorable) for the position of the unique sulfur atom in TFP. The remainder of each drug molecule is shown in light gray sticks. For each of the four CaM structures, CaM-TFP complexes calculated to have identical free energies are shown in the same color.

Results

The major aims of this study were to understand the allosteric effects of TFP on the domains of CaM by comparing the stoichiometry of TFP binding to apo and calcium-saturated domains of CaM, and determining thermodynamic effects of TFP on calcium-binding affinity.

TFP Titration of apo ^{15}N-PCaM

The stoichiometry of TFP binding to apo PCaM was determined using ^{15}N-HSQC spectra to examine changes in the local chemical environment of individual amide resonances as TFP was titrated into a solution of uniformly ^{15}N-labeled PCaM. The sample had been depleted of calcium via extensive dialysis against metal chelators.

In the absence of TFP, 126 resonances were identified for $PCaM_{1-148}$. TFP addition resulted in residue-specific perturbations of almost all of these resonances. Individual peaks found to be in fast exchange were tracked over the course of the TFP titration (a subset are shown in Fig. 2a-c). This analysis revealed that TFP saturated apo PCaM at a stoichiometry of 2:1. At saturation by TFP, resonances corresponding to the C-domain of PCaM showed a greater average degree of chemical shift perturbation (Δppm of 0.044) than those of the N-domain (Δppm of 0.030) (Fig. 2c). As shown in Fig. 2d, residues having significant backbone amide chemical shifts (Δppm ≥ 0.05) are mapped onto corresponding residues of a high resolution solution structure of apo CaM in its extended form [5,8].

The drug was observed to bind sequentially to the two domains of apo PCaM. The largest change in most resonances of the C-domain occurred in the range of 0 to 1 molar equivalents of TFP, whereas the largest change in most resonances of the N-domain occurred in the range between 1 and 2 molar equivalents of TFP. This indicated that TFP bound preferentially to the C-domain, despite the extensive similarity of the N- and C-domains in sequence and structure. A distinct subset of residues (~30%) responded continuously over the range of zero to 2 molar equivalents of TFP. That group included Phe16, Ile86, Thr110, and Gly113; their response is shown in Fig. 2b.

TFP Titration of $(Ca^{2+})_4$-^{15}N-PCaM

For calcium-saturated PCaM, 133 resonances were resolved. Saturation with TFP was reached at a rato pf 4:1 TFP:PCaM (Fig. 3). Over the course of the titration, 17 resonances experienced slow or intermediate exchange, with the majority (13) of these located in the C-domain of $(Ca^{2+})_4$-PCaM. Final chemical shift values due to TFP addition for these residues were not determined, because only ^{15}N-HSQC spectra were collected for this study. Therefore, it was not possible to determine Δppm. Their positions are represented by the absence of a bar in Fig. 3c.

Of the 116 resonances that were observed to be in fast exchange upon TFP addition, 98 were classified as being perturbed significantly (Δppm ≥ 0.05). They correlated closely with the location of TFP-binding sites observed in the crystallographic structure (1LIN.pdb) that showed 4 TFP bound to $(Ca^{2+})_4$-CaM (Fig. 3d). Although the calcium-binding sites of CaM are distant from the TFP-binding sites observed in all three of the crystal structures shown in Fig. 1, some of their resonances were perturbed also.

Part of each ^{15}N-HSQC spectrum collected for the first and last point of the titration is shown overlapped in Fig. 3a; representative titrations of individual residues are shown in Fig. 3b. Of the 98 peaks that could be tracked throughout the titration, there were 74 that shifted monotonically; approximately half of those were in each domain of CaM (35 in the N-domain *vs*. 39 in the C-domain). The remaining 24 resonances exhibited a biphasic response to TFP addition. Some examples are shown in Fig. 4a-c. Many of these residues were located at the interface between the N- and C-domains of CaM (Fig. 4d).

This analysis of TFP-induced chemical shifts in $(Ca^{2+})_4$-^{15}N-PCaM indicated that the TFP-binding sites were non-equivalent, and that some residues responded to TFP binding at more than one of its sites. Notably, some residues in the N-domain (e.g., Glu11 and Glu14) were among this group, even though the N-domain of calcium-saturated CaM has only been observed to have a single TFP-binding site.

Equilibrium Calcium Titration of $CaM_{1\text{-}148}$

To determine the effect of TFP on the affinity of calcium for CaM, equilibrium calcium titrations of $CaM_{1\text{-}148}$ were conducted in the presence of discrete molar ratios of TFP:CaM ranging from zero to eight. In the absence of TFP, calcium binding to sites I and II in the N-domain of $CaM_{1\text{-}148}$ was monitored by observing a decrease in intrinsic phenylalanine fluorescence intensity (Fig. 5a, blue) as described in *Materials and Methods*. Nonlinear least squares analysis according to a model-independent two-site (Adair) function (Eq 2) established a reference total free energy (ΔG_2) of -13.05 ± 0.06 kcal/mol (Table 1). An increase in intrinsic tyrosine fluorescence intensity was used to monitor calcium binding to sites III and IV in the C-domain of $CaM_{1\text{-}148}$ (Fig. 5b, blue). In the absence of TFP, the total free energy was -15.00 ± 0.06 kcal/mol (Table 1).

Effect of TFP on calcium binding to $CaM_{1\text{-}148}$

Calcium titrations of $CaM_{1\text{-}148}$ were conducted at molar ratios of 1:1 (green), 2:1 (red), 3:1 (black), 4:1 (cyan), and 8:1 (purple) TFP:$CaM_{1\text{-}148}$. In these titrations, there is no experimental signal that reports directly on the number of TFP molecules bound to CaM or the fractional population of the possible ligation states of TFP bound to apo and calcium-saturated CaM. Therefore, each set of titrations will be referred to by the known independent variable: the ratio of the final mols of TFP to mols of CaM.

The calcium affinity of sites I and II of $CaM_{1\text{-}148}$ decreased or increased depending upon the concentration of TFP (Fig. 5a). Of the TFP:$CaM_{1\text{-}148}$ ratios examined, a 1:1 ratio caused the

largest decrease (2.08 kcal/mol) in calcium affinity at sites I and II (apparent free energy of -10.97 kcal/mol; green bar in inset). Calcium affinity was diminished at ratios of 2:1 (red) and 3:1 (black), but the effects were less severe than the ratio of 1:1. The smallest decrease (0.58 kcal/mol) in apparent free energy of binding at sites I and II occurred at a ratio of 4:1 TFP:CaM_{1-148} (-12.47 kcal/mol, turquoise). In contrast, an 8:1 ratio reversed the effect and made calcium binding to sites I and II more favorable by -0.54 kcal/mol (relative to the binding affinity observed in the absence of TFP). This effect is represented by the bar graph inset in Fig. 5a showing values of $\Delta\Delta G_2$. Although small in absolute magnitude, this reversal is considered significant because the standard deviation of replicate measurements for all of these titrations ranged from 0.04 to 0.16 kcal/mol, and was much smaller than 0.54 kcal/mol.

The effects of TFP on calcium sites III and IV of CaM_{1-148} shared several features of its effects on sites in the N-domain. At all levels tested, TFP made calcium binding to sites III and IV of CaM_{1-148} less favorable. The pattern of effects (Fig. 5b) in response to an increasing ratio of TFP:CaM_{1-148} was similar to that observed for sites I and II (Fig. 5a). The bar graph inset shows that the free energy of -12.39 kcal/mol at a 1:1 TFP:CaM_{1-148} ratio represented the maximum change in ΔG_2 of 2.61 kcal/mol. At a ratio of 2:1, the effect was slightly smaller; ratios of 3:1 and 4:1 both caused a decrease of ~1.8 kcal/mol in the calcium affinity of sites III and IV. A TFP:CaM_{1-148} ratio of 8:1 had the smallest effect; the apparent ΔG_2 was -13.99 kcal/mol, representing a change of only 1 kcal/mol relative to the absence of TFP. In this set of titrations, the *Span* was positive for ratios of 0, 1:1, 2:1 TFP:CaM. At ratios above 2:1, the fluorescence intensity decreased in response to an increase in calcium. For ease of comparison of medians and slopes of the titration, the signal for the titrations conducted at ratios of 3:1, 4:1 and 8:1 TFP:CaM are shown inverted.

The domain-specific effects of TFP on calcium binding to CaM_{1-148} were complex, and suggested that the domains had intrinsic differences in affinity for TFP, and possibly stoichiometry of TFP binding. The NMR-monitored TFP titrations of CaM_{1-148} suggested that TFP might bind to an interface between domains, as well as a hydrophobic cleft in each domain. To attempt to simplify these linked binding processes, each half-CaM domain fragment (CaM_{1-80} and CaM_{76-148}) was studied independently. Each one contains a pair of EF-hands that retain (a) cooperative calcium binding energetics, and (b) secondary and tertiary stucture nearly identical to that of full-length CaM.

Effect of TFP on calcium binding to CaM_{1-80}

Equilibrium calcium titrations of the CaM_{1-80} fragment (N-domain) were performed to examine the effect that TFP has on the calcium affinity of sites I and II in the absence of the C-domain. Analysis of a calcium titration in the absence of TFP (Fig. 6a, blue) showed that the total free energy of ΔG_2 of calcium binding to sites I and II was -12.91 kcal/mol (Table 1)

As was observed for CaM_{1-148}, the effect of TFP on the apparent free energy of calcium binding to sites I and II changed in magnitude in a nonlinear manner between ratios of 1:1 and 8:1 TFP:CaM (Fig. 6a). At a ratio of 1:1, the apparent ΔG_2 was -11.12 kcal/mol, almost 2 kcal/mol less favorable than for CaM alone. This ratio of TFP: CaM_{1-80} induced a smaller change than had been observed for calcium binding to sites I and II of CaM_{1-148}. A TFP:CaM_{1-80} ratio of 2:1 reduced the calcium affinity further, such that ΔG_2 was -10.70 kcal/mol; this was the largest effect that TFP was observed to have on CaM_{1-80}, as shown in the bar graph inset of $\Delta\Delta G_2$ values in Fig. 6a. A TFP:CaM_{1-80} ratio of 3:1 had a slightly greater, but nearly identical effect, to a ratio of 4:1, consistent with its effect on sites I and II in CaM_{1-148} at these ratios. The most striking difference was observed at the ratio of 8:1 TFP:CaM. Calicum binding to sites I and II remained less favorable by 0.63 kcal/mol for

CaM_{1-80}. This indicated that the C-domain was necessary for the favorable effect (-0.54 kcal/mol) of TFP on sites I and II in CaM_{1-148} that had been observed at an 8:1 TFP:CaM ratio.

Effect of TFP on calcium binding to CaM_{76-148}

To examine the effect that TFP had on the calcium affinity of sites III and IV in the absence of the N-domain, the free energy of calcium binding to the pair of sites in CaM_{76-148} was determined. In the absence of TFP, ΔG_2 was determined to be -14.47 kcal/mol (Table 1) (Fig. 6b). A ratio of 1:1 TFP:CaM_{76-148} led to a decrease in affinity (the apparent ΔG_2 was less favorable by 1.67 kcal/mol). This was smaller than the change (2.56 kcal/mol) observed for calcium binding to the same sites in CaM_{1-148}. The difference of almost 1 kcal/mol is greater than the largest standard deviation (0.26 kcal/mol) observed for a single condition. The calcium-dependent change in fluorescent intensity was positive, as it was in the absence of TFP. However, the absolute magnitude of the intensity was lower (data not shown).

At ratios of 2:1 (red) and 3:1 (black) TFP:CaM_{76-148}, non-monotonic calcium-dependent changes in fluorescence intensity signals were observed. The first inflection was an increase in intensity, like that observed for calcium titrations conducted at a ratio of 1:1 TFP:CaM. Representative normalized data sets are shown in the insert of Fig. 6b. The second inflection was a decrease in intensity; both the first and second transitions are shown in the inset Fig. 6 for the ratios of 2:1 and 3:1. Apparent free energies were estimated using piece-wise analysis of the two transitions, as described below.

As shown in Fig. 6b, at ratios of 4:1 and 8:1 TFP:CaM_{76-148}, a greater decrease in the calcium affinity of sites III and IV was observed than had been seen at the same ratio of TFP:CaM for these sites in CaM_{1-148}. Presumably this relates to the absence of the N-domain and interdomain sites as locations for TFP binding. Also, as had been observed for CaM_{1-148}, the *Span* observed for the calcium-dependent change in fluorescence intensity was negative. For ease of comparing medians and slopes of the titrations, the normalized titrations at these two conditions were inverted in Fig. 6b. The slope of the calcium titration at a ratio of 8:1 TFP:CaM was notably more shallow than those at other molar ratios of TFP:CaM. This may arise from a change in cooperativity and/or may represent a mixed population of ligation states: CaM_{76-148} saturated with varying numbers of TFP.

Piecewise analysis of biphasic calcium titrations of CaM_{76-148}

The calcium titrations conducted at ratios of 2:1 and 3:1 TFP:CaM (Fig. 6 insert) are comprised of two phases with a sharp transition between them. Because the asymptotes for each phase were not well defined, it was not possible to determine an independent maximum for the upward-trending signal, or minimum for the downward-trending signal by fitting the data to Eq. 3.

Instead, to estimate the apparent free energy of calcium binding, the fluorescent signal was normalized to the maximal observed intensity, and the value of *Span* was set equal to 1.0. Using that approach, the apparent free energies of Ca^{2+} binding were -12.78 kcal/mol (at ratio of 2:1) and -13.02 kcal/mol at a ratio of 3:1. The corresponding estimates of $\Delta\Delta G_2$ for calcium binding to sites III and IV are shown in the solid bars in the inset of Fig. 6b. These values were similar to what had been observed at 1:1 TFP:CaM. (The maximal fluorescence intensity for the increasing phase must be at least as high the value observed, but could be higher. If it were under-estimated, this approach would also under-estimate the effect of TFP by estimating a median calcium concentration lower than the actual value and therefore closer to the value in the absence of TFP.)

A similar approach was applied to analysis of the decreasing signal recorded at ratios of 2:1 (red) and 3:1 (black) TFP:$CaM_{76\text{-}148}$. The net downward deflection was fixed to be as large as that for the increasing phase. Using this approach, the apparent free energies were -9.55 (a ratio of 2:1) and -10.65 kcal/mol (at 3:1). The dashed bars shown in the inset of Fig. 6b represent the value of $\Delta\Delta G_2$ values obtained assuming that the net change in affinity is equal to the effect represented by the decreasing fluorescent intensity. If the value of the *Span* of this transition were not as large as the increasing phase, this assumption would err on the side of reporting a weaker calcium-binding affinity (i.e., a median concentration for the titration that would be higher than the actual one).

The presence of multi-phasic fluorescence signals, changes in direction of calcium-depending response of steady-state fluorescence, and differing free energies of Ca^{2+} binding as a function of [TFP] provide strong evidence for the existence of populated intermediates that have different fluorescence signals. All estimates of calcium binding affinity in the presence of TFP are denoted as apparent free energies to draw attention to the complexity of analysis of multiple, partial ligation states.

Contrast between TFP-Binding Interfaces of apo and $(Ca^{2+})_4$-CaM

Evidence that TFP recognizes different surfaces of apo and $(Ca^{2+})_4$-CaM comes from comparing ^{15}N-HSQC spectra of TFP-saturated apo and $(Ca^{2+})_4$-CaM (Fig. 7a). The spectra differ at most positions, meaning that the local chemical environments of most amide bonds in the CaM backbone are non-equivalent. These changes appear to be considerably larger than those observed by Matsushima et al [43]; although, a direct comparison cannot be made because chemical shifts due to TFP binding were not quantified in that study.

It would be attractive to determine a high-resolution structural model of TFP bound to apo CaM which would reveal residues participating in the drug-protein interfaces and interhelical angles of each 4-helix bundle domain. However, it is beyond the scope of this study. Instead, a computational approach (*AutoDock Vina* [44]) was used to identify an ensemble of 20 preferred binding sites for TFP on the apo C-domain of CaM in a “closed”, “semi-open” and “open” conformation (Fig. 8a). Free energies of TFP bin

For the “closed” C-domain (based on 1DMO), the preferred binding locations of TFP were on the exterior surface near the first and second helix of the domain, and near the highly acidic calcium-binding sites III and IV; predicted free energies for this set of models ranged from -6 to -5.1 kcal/mol. The “semi-open” C-domain (based on 2IX7), showed two preferred binding locations: one was in the shallow cleft between the pairs of helices in the 4-helix bundle and the other was near site III. Free energies of TFP binding to the “semi-open” domain ranged from -6.8 to -6.0 kcal/mol.

The “open” C-domain has only been observed in structures of $(Ca^{2+})_4$-CaM. However, it may be sampled at a very low frequency by apo CaM. Therefore, TFP binding to an apo “open” C-domain was modeled by removing the calcium ions from two “open” tertiary structures of calcium-saturated CaM that differed in their sidechain orientations. One set of coordinates was taken from a structure of $(Ca^{2+})_4$-CaM bound to a peptide (2HQW) and another was from a structure of $(Ca^{2+})_4$-CaM bound to 4 TFP (1LIN). In both cases, the most favorable binding site for TFP was located deep in the hydrophobic pocket between the pairs of helices.

The “open” conformation is the only one for which there are high resolution structures showing the location(s) of TFP bound to the C-domain. The position of TFP at site A of 1LIN.pdb (see Fig. 1c) is shown in magenta for comparison to the models. This site is occupied in all three crystallographic structures of TFP bound to $(Ca^{2+})_4$-CaM. For the 20

models having the lowest energy, the sulfur atom in each computationally docked TFP molecule was within 1 Å of the location where it had been observed experimentally in 1LIN, suggesting that the interhelical angles and surface residues are necessary and sufficient to provide a binding site for TFP in the absence of calcium.

There are some caveats that should be noted. This prediction of sites of TFP binding to the "closed" and "semi-open" conformations of a single domain does not explore additional possible sites that might exist in full-length apo CaM in pockets created by the juxtaposition of the two domains. This is known to occur in a structure of 4 TFP bound to $(Ca^{2+})_4$-CaM (Fig. 7b). These calculations also do not take into account the energy required for isomerization between "closed", "semi-open" and "open" conformations of CaM. A barrier exists between these because the "open" form of each 4-helix bundle domain of $(Ca^{2+})_4$-CaM exposes more hydrophobic surface to solvent than the "closed" or "semi-open" conformations [8,17]. However, the models suggest that TFP binding to the "semi-open" form has the potential of interfering with calcium binding.

Discussion

The studies presented here address the nature of TFP binding to apo and calcium-saturated CaM, and the allosteric effects of TFP on calcium binding to the non-equivalent domains of CaM. Their combined effects on conformational switching of this essential regulatory protein are of interest because of the ubiquitous practice of applying drugs to cell cultures to disrupt CaM-mediated pathways of calcium-dependent signal transduction.

Two TFP molecules bind to apo CaM

Although some reports suggest that TFP binds to apo CaM [45 43];, most have not supported this premise [30,46,47]. In this study, stoichiometric TFP titrations of apo $CaM_{1\text{-}148}$ monitored by NMR showed saturation by two TFP molecules, with preferential binding to the C-domain. Studies of calcium binding to TFP-saturated apo CaM monitored by fluorescence demonstrated that TFP reduced calcium affinity. This was similar to the effect of peptides derived from individual protein targets, such as those containing IQ-motifs, that bind preferentially to apo CaM [15,16] and decrease the calcium-binding affinity of the EF-hand sites of CaM. However, to our knowledge, this is the first time such behavior has been reported for a drug binding to CaM.

In a unique high resolution study of apo CaM bound to a peptide representing an IQ-motif (from myosin V[17]), the C-domain of CaM is in the "semi-open" tertiary conformation (Fig. 2). The interface between the peptide and the "semi-open" C-domain buries more surface area than does interface between peptide and "closed" N-domain. In other structures of CaM:peptide complexes, the C-domain has been observed to adopt multiple conformations, depending on the nature and number of ligand(s) (calcium and/or protein) bound (Fig. 1b). In apo CaM alone, the C-domain has a lower fraction of ordered secondary structure and is less thermodynamically stable than the N-domain [4,48]. These findings for apo CaM indicate that fluctuation between a "closed" and "semi-open" conformation is more energetically favorable for the C-domain than for the N-domain, consistent with TFP binding preferentially to the C-domain. It is also possible for either apo N- or C-domain to sample the "open" conformation. However, favorable tertiary constraints within each domain provide an energetic barrier for this transition. Thus, the population of this conformation of apo CaM will be low.

Small-angle x-ray scattering (SAXS) data indicate that TFP binds to both apo and $(Ca^{2+})_4$-CaM. However, the radius of gyration of each ensemble is different [43,45] suggesting that the dominant tertiary structure and stoichiometry of TFP binding are not identical for apo and

$(Ca^{2+})_4$-CaM. Because both of these differ from apo CaM alone which preferentially populates the "closed" conformation, we hypothesize that TFP binds preferentially to the "semi-open" conformation of the 4-helix bundle domains of apo CaM. At a specific [TFP], the fraction of apo CaM having TFP bound to a "semi-open" domain will be determined by the energy of isomerization reactions needed for conformational rearrangements, the energy of TFP binding to CaM, and concentration of TFP.

Four TFP bind to $(Ca^{2+})_4$-CaM

Residue-specific titrations monitored by NMR (Fig. 3) showed the stoichiometry of TFP binding to $(Ca^{2+})_4$-CaM was 4:1 in agreement with a SAXS study [45], an HPLC study [46,28], and one of the three crystallographic structures 1LIN.pdb [49]. The stoichiometry of 4 contrasts with two other crystallographic structures of CaM:TFP (1CTR.pdb, 1A29.pdb, see Fig. 1c), and a recent computational study that concluded that TFP binds only to the C-domain of $(Ca^{2+})_4$-CaM [50]. Although NMR is a powerful method for determining stoichiometry of ligand binding, the observed spectral changes may arise from local binding, or a global conformational change making it challenging to determine the location of individual sites. TFP binding perturbed amide resonances in both domains of $(Ca^{2+})_4$-CaM, consistent with TFP binding to each per Fig. 1c (sites A, B, C, and D). The majority of residues in slow exchange mapped to the C-domain, indicating that this domain had the single site with highest affinity. Coupled with the locations of residues in both domains that undergo fast exchange, indicates that a hierarchy of 4 TFP-binding sites are present in $(Ca^{2+})_4$-CaM. Interpreted according to the positions of TFP in 1LIN.pdb, it appeared that two TFP binding sites with different affinities exist in the C-domain, that a third low-affinity site is present in the N-domain, and that a fourth site (also of low affinity) bridges the two domains (Fig. 7b). It was not possible to distinguish a preferential order of binding order to the low-affinity sites.

Interdomain Interactions

For any protein binding 4 ligands, there are 5 macroscopic ligation states (0, 1, 2, 3, 4 ligand:protein). Thus, in principle, it might be possible to titrate $(Ca^{2+})_4$-CaM with TFP and monitor 4 independent transitions corresponding to individual TFP-binding sites as has been done for calcium binding to 4 sites in CaM [41, 51,52]. For residues of CaM affected by a single TFP molecule, a monotonic transition between a "free" and "bound" state might be observed. For each residue that experienced only those two chemical environments, a stoichiometric titration would show (a) a linear transition, if in fast exchange, or (b) reciprocal changes in intensity for pairs of peaks (one diminishing, one increasing), if in slow exchange. Similarly, if there were 4 sites with identical affinity, all residues affected by TFP binding would titrate identically over the range of 0 to 4 equivalents of TFP added.

However, it is also possible that intermediate ligation states adopt distinct conformers with unique biophysical properties. A residue that responds to TFP binding at multiple sites has the potential to experience a different environment in each, and therefore show a nonlinear response to TFP binding as monitored by NMR or fluorescence. In HSQC spectra, the subset of residues (Fig. 4) that experienced at least three chemical environments and sampled at least one intermediate conformation are probably located at the interface between the N- and C-domains, or between TFP binding sites within a single domain (Fig. 4c). The crystallographic structure of 4 TFP molecules bound to $(Ca^{2+})_4$-CaM shows that, at their closest approach, TFP binding sites A, B, and C are in close proximity (~4 Å) to each other, while the TFP molecule bound at site D is ~9 Å away from site C (Fig. 7b). This constellation would allow unique chemical environments to be sampled as TFP sequentially fills 4 binding sites, and would change the chemical environment of adjacent TFP binding sites.

This type of biphasic response of CaM resonances was observed previously in ^{15}N-HSQC monitored calcium titrations of CaM [41] as well as in drug titrations of cardiac Troponin C (a related calcium-binding EF-hand protein) [53]. Nonlinear peak shifts due to the significant population of an intermediate state have also been observed for other proteins such as the phosphorylated kinase-inducible activation domain (pKID) of the transcription factor CREB binding KIX [54].

Further evidence for domain interactions was provided by the behavior of residues Glu11 and Glu 14. These residues were expected to respond to TFP binding to the N-domain based on their location and proximity to a target peptide or drug observed in 17 $(Ca^{2+})_4$-CaM-peptide or drug complexes [31]. In those, both Glu11 and Glu14 were within 4.5 Å of the peptide or drug interacting with $(Ca^{2+})_4$-CaM. Over the range of 0 to 4 TFP molecules binding to $(Ca^{2+})_4$-CaM, these residues exhibited a biphasic response to TFP binding (Fig. 4d), initially increasing to a maximum at 2 TFP:CaM. These residues are located between TFP-binding sites in the N- and C-domain of $(Ca^{2+})_4$-CaM which positions them to respond to saturation of all TFP binding sites. The highest affinity TFP-binding site in $(Ca^{2+})_4$-CaM is in the C-domain, assumed to be TFP-site A (Fig. 1c, Fig. 8a). Glu11 and Glu14 are also < 4 Å from TFP-site B which is comprised primarily of C-domain residues; their response from 0 to 2 may reflect occupancy of sites A and B, while the response from 2 to 4 indicates occupancy of sites C and D. But, other models of hierarchical binding are consistent with the titrations.

Effects of TFP on the Calcium Affinity of CaM

Similar to the IQ-motif of $Na_v1.2$ IQp, TFP diminished the calcium-binding affinity of both domains of CaM. TFP binds with lower absolute affinity to apo CaM [47] than does $Na_v1.2$ IQp [16]. However, like $Na_v1.2$ IQp, it has a higher relative affinity for the C-domain of apo CaM (Fig. 3) than for the N-domain which is consistent with the observation that the C-domain exhibited a larger TFP-induced decrease in calcium affinity (Fig. 5b). If $(Ca^{2+})_4$-CaM had not bound TFP at all, or bound TFP more weakly than apo CaM but at the same sites, then the major allosteric effect of TFP would be to decrease calcium affinity by binding preferentially to apo CaM. The magnitude of the TFP effect would increase monotonically until CaM was saturated with TFP. In this way, its effect on CaM would be analogous to that of 2,3-BPG reducing oxygen binding affinity by binding preferentially to deoxy hemoglobin [55-57]. However, this mechanism of negative allosteric regulation would not explain how the effect of TFP reversed direction (Figs. 5 and 6) as the ratio of TFP:CaM increased to 8. Several explanations were considered.

The reversal of the initially negative allosteric effect of TFP might be explained if higher levels of total added TFP did not actually represent higher soluble concentrations. The effective [TFP] might drop if it formed micelles that would compete with CaM as a sink for additional TFP. However, that model contradicts several observations. For example, a prediction would be that increasing TFP would ameliorate the initially negative effect until all of it was drawn into micelles and the calcium-binding affinity of CaM returned to that observed in the absence of TFP. Instead, an increase in TFP ultimately increased the calcium-binding affinity of CaM, rather than returning it to the values in the absence of TFP. An additional contrary observation was that the direction of calcium-dependent changes in fluorescence signal changed over the course of the TFP titration: monotonically increasing in the absence of TFP, and monotonically decreasing at the 8:1 ratio, showing that TFP was still associated with CaM at the 8:1 ratio. Finally, in all CaM-TFP samples (including the millimolar CaM samples used in NMR studies), there was no visual evidence of turbidity that would indicate the formation of micelles.

Another possibility is that the mechanism of allosteric reversal depends on TFP changing the relative populations of “closed”, “semi-open”, and “open” tertiary stuctures of apo CaM. Given that both calcium and TFP have micromolar affinity for CaM, and that two calcium ions are needed to drive each domain to adopt the “open” state in the absence of TFP, it may be that 2 TFP molecules are needed to drive the conformational change of opening each domain. The NMR-monitored TFP titrations showed only two TFP bound to apo $CaM_{1\text{-}148}$, but they did so sequentially with higher affinity for the C-domain. In contrast, multiple TFP may bind cooperatively to “open” calcium-saturated domains. Thus, as the level of TFP increases above 1:1, there is a chance for more than 1 to bind to a single domain. TFP may promote the “open” conformation of apo CaM by acting in a manner similar to that of BAA-motif peptides that bind with high affinity to the hydrophobic surfaces exposed upon Ca^{2+}binding [31,58]. That would then increase calcium-binding affinity. This biphasic binding shares some features with that observed for an IQ-motif from neuromodulin studied by Persechini and colleagues [59].

Comparison of the calcium-binding free energies for sites I and II in $CaM_{1\text{-}148}$ and $CaM_{1\text{-}80}$ at a ratio of 8:1 TFP:CaM revealed that unlike $CaM_{1\text{-}148}$, the calcium affinity of $CaM_{1\text{-}80}$ does not become more favorable than observed in the absence of TFP. This difference may result from the loss of a TFP-binding site that bridges the N- and C-domains of $CaM_{1\text{-}148}$ (Fig. 7b). Calcium titrations of $CaM_{76\text{-}148}$ at ratios of 2:1 and 3:1 TFP:$CaM_{76\text{-}148}$ resulted in multiphasic fluorescence signals attributed to a mix of different TFP-bound $CaM_{76\text{-}148}$, complexes that each have unique properties. This is consistent with kinetic studies of calcium release from $(Ca^{2+})_4$-CaM mixed with TFP [60]. Different species in solution are sufficiently populated at ratios of 2:1 and 3:1 TFP:$CaM_{76\text{-}148}$ to exhibit multiple signals, but are not abundant at the ratios of 1:1, 4:1, and 8:1. For ratios of 2:1 and 3:1, the maximum value of raw intensity was approximately a third of that observed for the calcium titrations conducted at 1:1 and 4:1 ratios of TFP:$CaM_{76\text{-}148}$. These data are consistent with a mechanism in which the apo C-domain has a higher affinity for TFP than does the apo N-domain, and that TFP binding interferes with calcium binding by inhibiting the switch from “semi-open” to “open” conformation.

These interpretations are summarized in a simplified isomerization and binding model shown in Fig. 8b. Distinct tertiary conformations of CaM provide unique TFP binding interfaces with different relative affinities for TFP. A “closed” domain of apo CaM does not bind TFP. A “semi-open” apo domain has hydrophobic residues (shown as blue patches) that interact with TFP in a manner similar to interactions with the Ile-Gln dipeptide in a canonical IQ-motif. Calcium binding is sufficient to switch the tertiary structure from the “semi-open” to “open” conformation, exposing hydrophobic residues (lavender) located deep in the hydrophobic cleft. The “open” conformation may be sampled transiently by apo CaM, allowing TFP at high concentrations to bind and have an allosteric effect on calcium affinity more like that of a BAA motif peptide which consistently buries an aromatic group in the FLMM pocket of the C-domain [31,61]. But, because the semi-open conformation would be abundant at low stoichiometries of TFP:CaM, its primary effect would to lower calcium affinity. Binding deep in the pocket would be enhanced by a second or third TFP binding to CaM.

Physiological Consequences of TFP Exposure

This study of the allosteric regulation of calcium binding to CaM by TFP demonstrates that there is considerable complexity in the interactions between these two ligands of CaM. TFP interacts with distinct interfaces available in the dominant tertiary conformations of apo and $(Ca^{2+})_4$-CaM. TFP titrations monitored by NMR showed differences in the stoichiometry and location of binding of TFP to apo and $(Ca^{2+})_4$-CaM; this is the driving force behind the non-monotonic allosteric effect of TFP on the calcium affinity of CaM.

This analysis suggests that despite the significant number of calcium-dependent processes regulated by $(Ca^{2+})_4$-CaM, it is equally important to consider interactions of target proteins with apo CaM when testing lipophilic drugs similar to TFP. This broadens the interpretation of a widely used approach of bathing cells *in vitro* in a TFP-containing solution (~1 μM – 30 μM) with the goal of disrupting pathways that are regulated by $(Ca^{2+})_4$-CaM [62,63].

Like other anti-psychotic drugs, TFP can cause the debilitating side-effect of tardive dyskinesia [64]. The etiology of this is not completely understood, but believed to originate from hypersensitive dopamine receptors, which have been shown to be regulated by CaM under both apo and calcium-saturating conditions [65,66]. Apo and $(Ca^{2+})_4$-CaM have also been shown to regulate numerous ion channels responsible for the propagation of nerve impulses [31,67-69]. It is possible that TFP alters physiological processes by disrupting interactions of apo CaM with these receptors.

Given the large number of signaling pathways that CaM regulates, CaM itself is not a promising target for drug design. However, an interface between CaM and a particular target may offer more selectivity. This study of allosteric interactions between calcium and TFP suggests that interactions between channels and the “semi-open” form of CaM may be an especially attractive target for future drug testing.

Acknowledgments

We thank Ching Kung and coworkers for providing the JM109 bacterial over-expression vector for PCaM. We thank Santhana Velupillai and the University of Iowa Central NMR Facility for help with preliminary NMR experiments as well as Audra Hoffman, Nicole Housley, T. Idil Apak Evans and Rhonda Newman for preliminary studies of TFP-CaM interactions. We thank Warren DeLano and colleagues (*PyMol*, DeLano Scientific), and Oleg Trott, Arthur Olson and colleagues (*AutoDock Vina*, The Scripps Research Institute) who have made their software accessible to the scientific community.

Supported by the National Institutes of Health (RO1 GM 57001) to M.A.S., by a University of Iowa Center for Biocatalysis and Bioprocessing Fellowship and American Heart Association Predoctoral Fellowship to S.E.O., and by the Roy J. Carver Charitable Trust Grant 01-224.

Abbreviations

BAA	Basic Amphipathic α-helix
CaM	calmodulin
CaMKII	CaM-dependent Kinase II
EGTA	Ethylene glycol bis(α-aminoethyl ether)-N, N, N’, N’-tetraacetic acid
HEPES	N-(2-hydroxy-ethyl)piperazine-N’-2-ethanesulfonic acid
^{15}N-HSQC	Heteronuclear single quantum correlation
FLMM	F19/F92, L32/L105, M51/M124, and M71/M144 of CaM
NMDA	N-methyl D-aspartate receptor
PCaM	*Paramecium* calmodulin
PCaM$_{1—148}$	*Paramecium* calmodulin full-length, residues 1-148
PCaM$_{1—80}$	*Paramecium* calmodulin N-domain fragment, residues 1-80
PCaM$_{76—148}$	*Paramecium* calmodulin C-domain fragment, residues 76-148
TFP	Trifluoperazine
VDSC	Voltage-dependent sodium channel

References

1. Hidaka H, Ishikawa T. Molecular pharmacology of calmodulin pathways in the cell functions. Cell Calcium. 1992; 13:465–472. [PubMed: 1505008]
2. Newman RA, Van Scyoc WS, Sorensen BR, Jaren OR, Shea MA. Interdomain coopertivity of calmodulin to melittin preferentially increases calcium affinity of sites I and II. Proteins: Structure, Function, and Bioinformatics. 2008; 71(4):1792–1812.
3. Sorensen BR, Faga LA, Hultman R, Shea MA. Interdomain linker increases thermostability and decreases calcium affinity of calmodulin N-domain. Biochemistry. 2002; 41(1):15–20. [PubMed: 11771998]
4. Sorensen BR, Shea MA. Interactions between domains of apo calmodulin alter calcium binding and stability. Biochemistry. 1998; 37:4244–4253. [PubMed: 9521747]
5. Zhang M, Tanaka T, Ikura M. Calcium-induced conformational transition revealed by the solution structure of apo calmodulin. Nature Struct Biol. 1995; 2:758–767. [PubMed: 7552747]
6. Seamon KB. Calcium- and Magnesium-Dependent Conformational States of Calmodulin As Determined by Nuclear-Magnetic Resonance. Biochemistry. 1980; 19:207–215. [PubMed: 7352978]
7. VanScyoc WS, Sorensen BR, Rusinova E, Laws WR, Ross JB, Shea MA. Calcium binding to calmodulin mutants monitored by domain-specific intrinsic phenylalanine and tyrosine fluorescence. Biophysical Journal. 2002; 83(5):2767–2780. [PubMed: 12414709]
8. Kuboniwa H, Tjandra N, Grzesiek S, Ren H, Klee CB, Bax A. Solution structure of calcium-free calmodulin. Nature Struct Biol. 1995; 2:768–776. [PubMed: 7552748]
9. Meador WE, Means AR, Quiocho FA. Target enzyme recognition by calmodulin: 2.4 Å Structure of a calmodulin-peptide complex. Science. 1992; 257:1251–1255. [PubMed: 1519061]
10. Chattopadhyaya R, Meador WE, Means AR, Quiocho FA. Calmodulin Structure Refined at 1.7 Å Resolution. Journal of Molecular Biology. 1992; 228(4):1177–1192. [PubMed: 1474585]
11. Wilson MA, Brunger AT. The 1.0 Å Crystal Structure of Ca^{2+} -bound Calmodulin: an Analysis of Disorder and Implications for Functionally Relevant Plasticity. Journal of Molecular Biology. 2000; 301(5):1237–1256. [PubMed: 10966818]
12. Yap KL, Ames JB, Swindells MB, Ikura M. Diversity of conformational states and changes within the EF-hand protein superfamily. Proteins. 1999; 37(3):499–507. [PubMed: 10591109]
13. Wall ME, Clarage JB, Phillips GN. Motions of calmodulin characterized using both Bragg and diffuse X-ray scattering. Structure. 1997; 5(12):1599–1612. [PubMed: 9438860]
14. Cox JA. Interactive properties of calmodulin. BiochemJ. 1988; 249:621–629. [PubMed: 3281652]
15. Martin SR, Bayley PM. Calmodulin bridging of IQ motifs in myosin-V. FEBS Letters. 2004; 567:166–170. [PubMed: 15178316]
16. Theoharis NT, Sorensen BR, Theisen-Toupal J, Shea MA. The Neuronal Voltage-Dependent Sodium Channel Type II IQ Motif Lowers the Calcium Affinity of the C-Domain of Calmodulin. Biochemistry. 2008; 47(1):112–123. [PubMed: 18067319]
17. Houdusse A, Gaucher JF, Krementsova E, Mui S, Trybus KM, Cohen C. Crystal structure of apo-calmodulin bound to the first two IQ motifs of myosin V reveals essential recognition features. Proc Natl Acad Sci U S A. 2006; 103(51):19326–19331. [PubMed: 17151196]
18. Vandonselaar M, Hickie RA, Quail JW, Delbaere LTJ. Trifluoperazine-induced conformational change in Ca^{2+}-calmodulin. Nature Structural Biology. 1994; 1(11):795–801.
19. Vertessy BG, Harmat V, Bocskei Z, Naray-Szabo G, Orosz F, Ovadi J. Simultaneous binding of drugs with different chemical structures to Ca^{2+}-calmodulin: crystallographic and spectroscopic studies. Biochemistry. 1998; 37(44):15300–15310. [PubMed: 9799490]
20. Cook WJ, Walter LJ, Walter MR. Drug Binding by Calmodulin: Crystal Structure of a Calmodulin-Trifluoperazine Complex. Biochemistry. 1994; 33:15259–15265. [PubMed: 7803388]
21. Tang L, Shukla PK, Wang ZJ. Trifluoperazine, an orally available clinically used drug, disrupts opioid antinociceptive tolerance. Neurosci Lett. 2006; 397(1-2):1–4. [PubMed: 16380209]
22. Frankfurt OS, Sugarbaker EV, Robb JA, Villa L. Synergistic induction of apoptosis in breast cancer cells by tamoxifen and calmodulin inhibitors. Cancer Lett. 1995; 97:149–154. [PubMed: 7497456]

23. Chen Y, Pawar P, Pan G, Ma L, Liu H, McDonald JM. Calmodulin binding to the Fas-mediated death-inducing signaling complex in cholangiocarcinoma cells. J Cell Biochem. 2008; 103(3): 788–799. [PubMed: 17654480]
24. Barrington M, Majewski H. Trifluoperazine and calmidazolium have multiple actions on the release of noradrenaline from sympathetic nerves of mouse atria. Naunyn Schmiedebergs ArchPharmacol. 1994; 349:133–139.
25. Clapperton JA, Martin SR, Smerdon SJ, Gamblin SJ, Bayley PM. Structure of the Complex of Calmodulin with the Target Sequences of Calmodulin-Dependent Protein Kinase I: Studies of the Kinase Activation Mechanism. Biochemistry. 2002; 41:14669–14679. [PubMed: 12475216]
26. Heidorn DB, Seeger PA, Rokop SE, Blumenthal DK, Means AR, Crespi H, Trewhella J. Changes in the Structure of Calmodulin Induced by a Peptide Based on the Calmodulin-Binding Domain of Myosin Light Chain Kinase. Biochemistry. 1989; 28:6757–6764. [PubMed: 2790029]
27. Ikura M, Barbato G, Klee CB, Bax A. Solution structure of calmodulin and its complex with a myosin light chain kinase fragment. Cell Calcium. 1992; 13:391–400. [PubMed: 1505004]
28. Massom L, Lee H, Jarrett HW. Trifuoperazine binding to porcine brain calmodulin and skeletal muscle troponin C. Biochemistry. 1990; 29(3):671–681. [PubMed: 2110826]
29. Craven CJ, Whitehead B, Jones SK, Thulin E, Blackburn GM, Waltho JP. Complexes formed between calmodulin and the antagonists J-8 and TFP in solution. Biochemistry. 1996; 35(32): 10287–10299. [PubMed: 8756684]
30. Tanokura M, Yamada K. Effects of trifluoperazine on calcium binding by calmodulin. J Biol Chem. 1985; 260:8680–8682. [PubMed: 4019446]
31. Ataman ZA, Gakhar L, Sorensen BR, Hell JW, Shea MA. The NMDA Receptor NR1 C1 Region Bound to Calmodulin: Structural Insights into Functional Differences between Homologous Domains. Structure. 2007; 15(12):1603–1617. [PubMed: 18073110]
32. Pedigo S, Kephart CR, Shea MA. Cooperative Calcium Binding by Calmodulin as Probed by Endoproteinase Glu-C. BiophysJ. 1992; 61:A211.
33. Putkey JA, Slaughter GR, Means AR. Bacterial expression and characterization of proteins derived from the chicken calmodulin cDNA and a calmodulin processed gene. Journal of Biological Chemistry. 1985; 260(8):4704–4712. [PubMed: 2985564]
34. Beaven GH, Holiday ER. Ultraviolet absorption spectra of proteins and amino acids. Advances in Protein Chemistry. 1952; 7:319–386. [PubMed: 14933256]
35. Hart RC, Bates MD, Cormier MJ, Rosen GM, Conn PM. Synthesis and Characterization of Calmodulin Antagonistic Drugs. Methods Enzymol. 1983; 102:195–205. [PubMed: 6645970]
36. Johnson ML, Frasier SG. Nonlinear least-squares analysis. Methods Enzymol. 1985; 117:301–342.
37. Johnson ML, Correia JJ, Yphantis DA, Halvorson HR. Analysis of Data From the Analytical Ultracentrifuge by Nonlinear Least-Squares Techniques. BiophysJ. 1981; 36:575–588. [PubMed: 7326325]
38. Levin RM, Weiss B. Binding of trifluoperazine to the calcium-dependent activator of cyclic nucleotide phosphodiesterase. Molecular Pharmacology. 1977; 13:690–697. [PubMed: 18661]
39. Delaglio F, Grzesiek S, Vuister GW, Zhu G, Pfeifer J, Bax A. NMRPipe: a multidimensional spectral processing system based on UNIX pipes. J Biomol NMR. 1995; 6(3):277–293. [PubMed: 8520220]
40. Goddard, TD.; Kneller, DG. SPARKY. 3. University of California; San Francisco:
41. Jaren OR, Kranz JK, Sorensen BR, Wand AJ, Shea MA. Calcium-Induced Conformational Switching of Paramecium Calmodulin: Changes in the Protein Backbone Observed by Heteronuclear NMR Studies. Biochemistry. 2002; 41(48):14158–14166. [PubMed: 12450379]
42. Trott O, Olson AJ. AutoDock Vina: Improving the speed and accuracy of docking with a new scoring function, efficient optimization, and multithreading. J Comput Chem. 2009; 31(2):455–461. [PubMed: 19499576]
43. Matsushima N, Hayashi N, Watanabe N, Jinbo Y, Izumi Y. Binding of trifluoperazine to apocalmodulin revealed by a combination of small-angle X-ray scattering and nuclear magnetic resonance. Journal of Applied Crystallography. 2007; 40:S179–S183.

44. Trott O, Olson AJ. AutoDock Vina: Improving the speed and accuracy of docking with a new scoring function, efficient optimization, and multithreading. J Comput Chem. 31(2):455–461. [PubMed: 19499576]
45. Matsushima N, Hayashi N, Jinbo Y, Izumi Y. Ca^{2+}-bound calmodulin forms a compact globular structure on binding four trifluoperazine molecules in solution. Biochem J. 2000; 347(Pt 1):211–215. [PubMed: 10727421]
46. Massom LR, Lukas TJ, Persechini A, Kretsinger RH, Watterson DM, Jarrett HW. Trifluoperazine binding to mutant calmodulins. Biochemistry. 1991; 30(3):663–667. [PubMed: 1988054]
47. Massom L, Lee H, Jarrett HW. Trifluoperazine binding to porcine brain calmodulin and skeletal muscle troponin C. Biochemistry. 1990; 29(3):671–681. [PubMed: 2110826]
48. Masino L, Martin SR, Bayley PM. Ligand binding and thermodynamic stability of a multidomain protein, calmodulin. Protein Science. 2000; 9(8):1519–1529. [PubMed: 10975573]
49. Vandonselaar M, Hickie RA, Quail JW, Delbaere LT. Trifluoperazine-induced conformational change in Ca(2+)-calmodulin. Nat Struct Biol. 1994; 1(11):795–801. [PubMed: 7634090]
50. Kovesi I, Menyhard DK, Laberge M, Fidy J. Interaction of antagonists with calmodulin: insights from molecular dynamics simulations. J Med Chem. 2008; 51(11):3081–3093. [PubMed: 18459732]
51. Martin SR, Linse S, Bayley PM, Forsen S. Kinetics of Cadmium and Terbium Dissociation from Calmodulin and Its Tryptic Fragments. Eur J Biochem. 1986; 161(3):595–601. [PubMed: 3792310]
52. Starovasnik MA, Su DR, Beckingham K, Klevit RE. A series of point mutations reveal interactions between the calcium-binding sites of calmodulin. Protein Science. 1992; 1(2):245–253. [PubMed: 1363934]
53. Kleerekoper Q, Liu W, Choi D, Putkey JA. Identification of binding sites for bepridil and trifluoperazine on cardiac troponin C. J Biol Chem. 1998; 273(14):8153–8160. [PubMed: 9525919]
54. Sugase K, Dyson HJ, Wright PE. Mechanism of coupled folding and binding of an intrinsically disordered protein. Nature. 2007; 447(7147):1021–1025. [PubMed: 17522630]
55. Benesch R, Benesch RE. The effect of organic phosphates from the human erythrocyte on the allosteric properties of hemoglobin. Biochem Biophys Res Commun. 1967; 26(2):162–167. [PubMed: 6030262]
56. Arnone A. X-ray Diffraction Study of Binding of 2,3-diphosphoglycerate to Human Deoxyhaemoglobin. Nature. 1972; 237:146–149. [PubMed: 4555506]
57. Ackers GK. Linked Functions in Allosteric Proteins: An Exact Theory for the Effect of Organic Phosphates on Oxygen Affinity of Hemoglobin. Biochemistry. 1979; 15:3372–3380. [PubMed: 465477]
58. Meador WE, Means AR, Quiocho FA. Modulation of calmodulin plasticity in molecular recognition on the basis of X-ray structures. Science. 1993; 262:1718–1721. [PubMed: 8259515]
59. Black DJ, Leonard J, Persechini A. Biphasic Ca2+-dependent switching in a calmodulin-IQ domain complex. Biochemistry. 2006; 45(22):6987–6995. [PubMed: 16734434]
60. Martin SR, Andersson-Teleman A, Bayley PM, Drakenberg T, Forsén S. Kinetics of calcium dissociation from calmodulin and its tryptic fragments A stopped-flow fluorescence study using Quin 2 reveals a two-domain structure. EurJBiochem. 1985; 151:543–550.
61. Yamniuk AP, Vogel HJ. Calmodulin's flexibility allows for promiscuity in its interactions with target proteins and peptides. Molecular Biotechnology. 2004; 27:33–57. [PubMed: 15122046]
62. Oruch R, Hodneland E, Pryme IF, Holmsen H. Psychotropic drugs interfere with the tight coupling of polyphosphoinositide cycle metabolites in human platelets: a result of receptor-independent drug intercalation in the plasma membrane? Biochim Biophys Acta. 2008; 1778(10):2165–2176. [PubMed: 18503745]
63. Lee CS, Han ES, Han YS, Bang H. Differential effect of calmodulin antagonists on MG132-induced mitochondrial dysfunction and cell death in PC12 cells. Brain Res Bull. 2005; 67(3):225–234. [PubMed: 16144659]

64. Lahti RA, Evans DL, Stratman NC, Figur LM. Dopamine D4 versus D2 receptor selectivity of dopamine receptor antagonists: possible therapeutic implications. Eur J Pharmacol. 1993; 236(3): 483–486. [PubMed: 8102973]

65. Liu Y, Buck DC, Macey TA, Lan H, Neve KA. Evidence that calmodulin binding to the dopamine D2 receptor enhances receptor signaling. J Recept Signal Transduct Res. 2007; 27(1):47–65. [PubMed: 17365509]

66. Woods AS, Marcellino D, Jackson SN, Franco R, Ferre S, Agnati LF, Fuxe K. How calmodulin interacts with the adenosine A(2A) and the dopamine D(2) receptors. J Proteome Res. 2008; 7(8): 3428–3434. [PubMed: 18590318]

67. van Petegem F, Chatelain FC, Minor DL Jr. Insights into voltage-gated calcium channel regulation from the structure of the $Ca_{(V)}1.2$ IQ domain-Ca^{2+}/calmodulin complex. Nature Structural and Molecular Biology. 2005; 12:1108–1115.

68. Shah VN, Wingo TL, Weiss KL, Williams CK, Balser JR, Chazin WJ. Calcium-dependent regulation of the voltage-gated sodium channel hH1: intrinsic and extrinsic sensors use a common molecular switch. Proc Natl Acad Sci U S A. 2006; 103(10):3592–3597. [PubMed: 16505387]

69. Schumacher MA, Crum M, Miller MC. Crystal structures of apocalmodulin and an apocalmodulin/SK potassium channel gating domain complex. Structure. 2004; 12:849–860. [PubMed: 15130477]

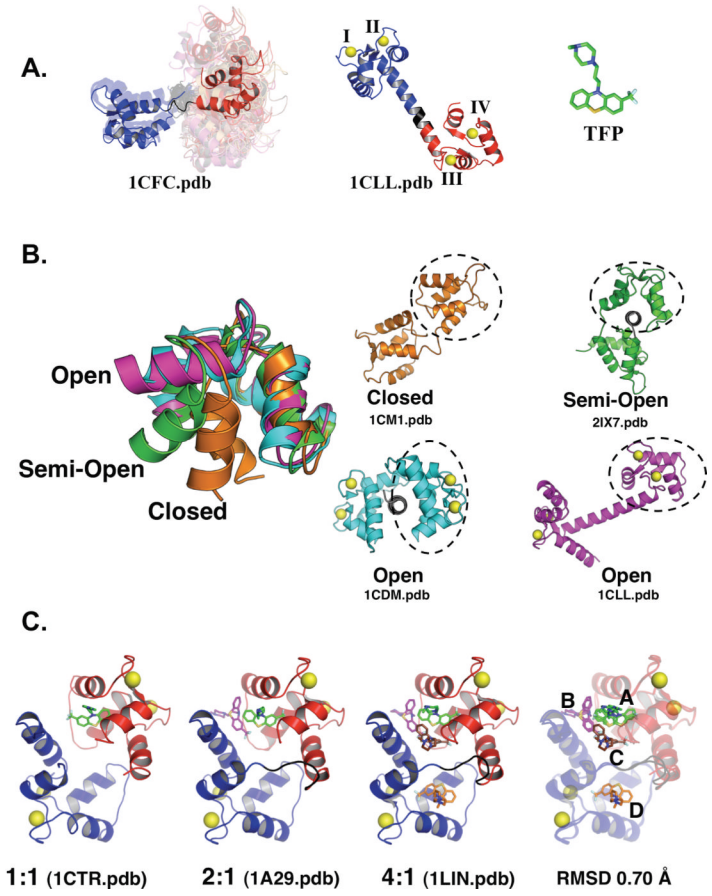

Figure 1. Structural Background of CaM-Target Interactions

A: Superposition of models of the solution structures of CaM (1CFC.pdb) that have been determined by NMR. Left: Alignment minimized the difference between models with respect to the N-domain (residues 1-75 in blue), illustrating the flexibility of the interdomain linker (resides 76-80 in black) and range of relative positions adopted by the C-domain (residues 81-148 in red). A single model is highlighted to reveal the tertiary structures of the apo N- and C-domains (each is a 4-helix bundle).

Middle: $(Ca^{2+})_4$-CaM structure determined crystallographically (1CLL.PDB); backbone colored as in panel A. Ca^{2+} ions (yellow) are bound at sites I and II in the N-domain, and at sites III and IV in the C-domain.

Right: Chemical structure of the antipsyschotic drug Trifluoperazine (TFP; green), with sulfur atom in yellow and fluorine atoms in light blue. Figure created with Pymol™.

B: Superposition of 3 Tertiary Structures of the C-domain of CaM.

Examples of the “closed” (1CFC.pdb–orange), “semi-open” (2IX7.pdb–green) and “open” (1CDM.pdb–aqua and 1CLL.pdb–magenta) conformations of the C-domain of CaM are aligned according to the positions of the F and G (second and third) helices of the domain. Structures of the corresponding full-length CaM is shown below. Figure created with Pymol™.

C: Structures of $(Ca^{2+})_4$-CaM bound to TFP.

Individual panels show crystallographically derived structures of TFP:$(Ca^{2+})_4$-CaM complexes, with drug:protein ratios of 1:1 (1CTR.pdb), 2:1 (1A29.pdf), and 4:1 (1LIN.pdb), as well as a structural superposition of these three structures, with the TFP-binding sites labeled A (green), B (magenta), C (brown) and D (orange). TFP-binding sites A and B are

located in the C-domain (backbone red), site C bridges the two domains, and site D is located in the N-domain (backbone blue). Figure created with Pymol™.

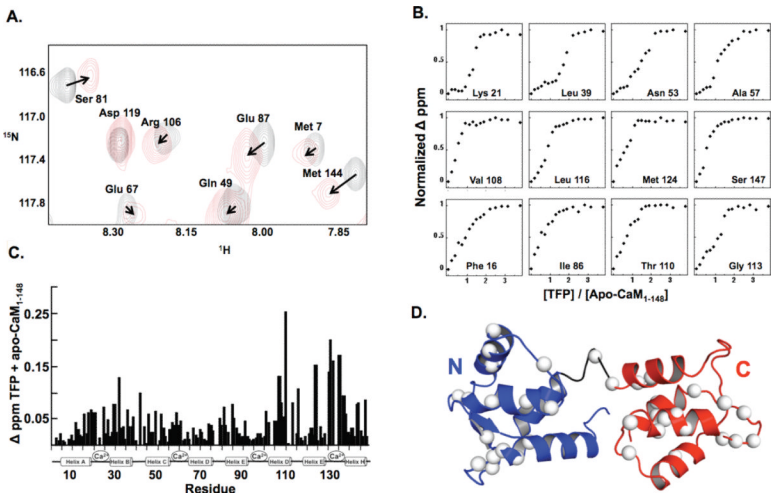

Figure 2. **^{15}N-HSQC-monitored TFP titration of uniformly ^{15}N-labeled apo PCaM**

A: Comparison of subset of ^{15}N-HSQC spectra for apo PCaM (black) and TFP-saturated apo PCaM (red); arrows indicate change in resonance positions over the course of the TFP titration. **B**: Normalized TFP-induced chemical shifts of individual representative residues of apo CaM. **C**: Bar graph of net chemical shift per residue caused by TFP saturation of CaM. **D**: Location of each apo CaM residue whose chemical shift was perturbed > 0.05 ppm by TFP saturation (white spheres); backbone modeled as that of apo CaM (1DMO.pdb). Solution conditions: 10% D_2O, 10 mM imidazole, 100 mM KCl, 50 μM EDTA, 5mM, pH 6.5 at 22°C. Figure created with Pymol™.

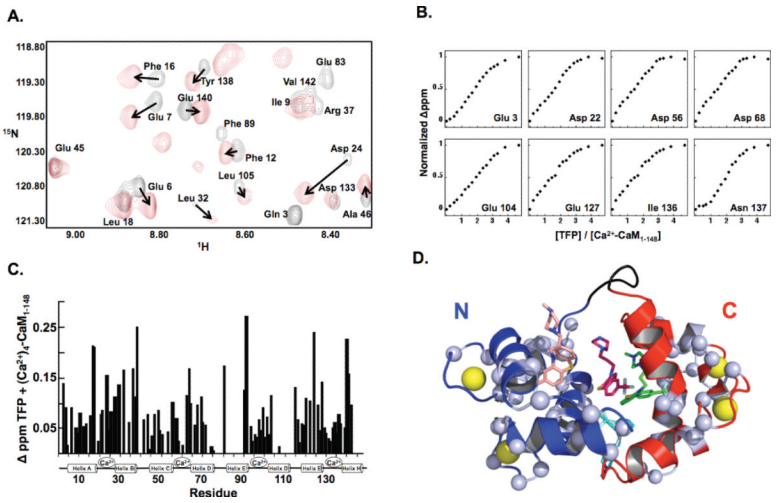

Figure 3. ^{15}N-HSQC-monitored TFP titration of uniformly ^{15}N-labeled $(Ca^{2+})_4$-CaM

A: Comparison of $(Ca^{2+})_4$-CaM (black) and TFP-saturated $(Ca^{2+})_4$-CaM (red) ^{15}N-HSQC spectra, arrows indicate change in resonance positions over the course of the TFP titration. **B**: Normalized TFP-induced chemical shifts of individual representative residues of $(Ca^{2+})_4$-CaM. **C**: Bar graph of net chemical shift per residue caused by TFP saturation of CaM. **D**: Location of each $(Ca^{2+})_4$-CaM residue whose chemical shift was perturbed > 0.05 ppm by TFP saturation (white spheres); backbone modeled according to the structure of TFP bound to $(Ca^{2+})_4$-CaM at a 4:1 ratio (1LIN.pdb). Solution conditions: 10% D_2O, 10 mM imidazole, 100 mM KCl, 50 μM EDTA, 5mM $CaCl_2$, pH 6.5 at 22°C. Figure created with Pymol™.

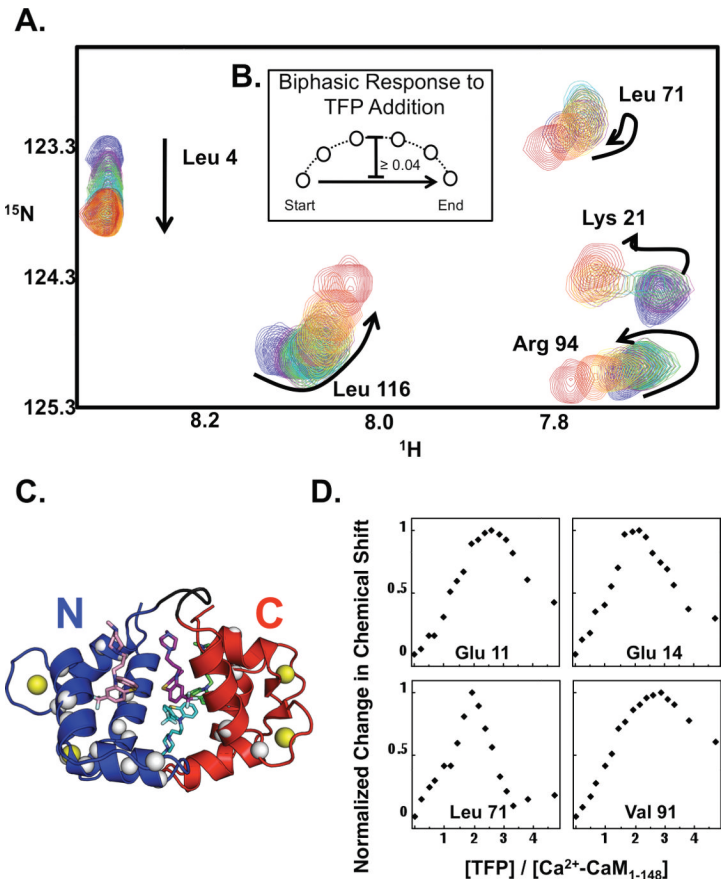

Figure 4. Multiple chemical environments observed upon TFP titration of $(Ca^{2+})_4$-CaM

A: ^{15}N-HSQC spectrum of uniformly ^{15}N labeled $(Ca^{2+})_4$-CaM titrated with TFP, where arrows represent the movement of each resonance from its initial position.

B: Schematic diagram of quantitative criterion for classification of biphasic chemical shift.

C: Locations of select residues that underwent a biphasic response upon TFP addition, mapped onto the structure of TFP bound to $(Ca^{2+})_4$-CaM at a 4:1 ratio (1LIN.pdb).

D: Normalized chemical shift plots for select individual residues deemed to undergo a biphasic response upon TFP titration of $(Ca^{2+})_4$-CaM. Solution conditions: 10% D_2O, 10 mM imidazole, 100 mM KCl, 50 μM EDTA, 5mM $CaCl_2$, pH 6.5 at 22°C. Figure created with Pymol™.

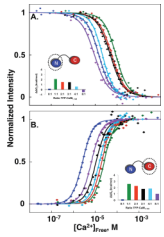

Figure 5. Effect of TFP on Calcium Binding to CaM_{1-148}

Equilibrium calcium titrations of CaM (6 μM) were conducted in the presence of 0 (blue), 6 (green, 1:1), 12 (red, 2:1), 18 (black, 3:1), 24 (cyan, 4:1), or 48 μM (purple, 8:1 TFP:CaM) TFP, and were monitored using the intrinsic fluorescence of CaM.

A: phenylalanine fluorescence (250 nm_{ex} and 280 nm_{em}).

B: tyrosine fluorescence (277 nm_{ex} and 320 nm_{em}). In B, for 3:1, 4:1 and 8:1 TFP:CaM, the raw signal decreased; it is shown inverted to facilitate comparisons.

Solid curves were simulated according to Eq. 3 and free energies in Table 1; bar graph insets represent $\Delta\Delta G_2$ values in Table 1. Solution conditions: 50 mM HEPES, 100 mM KCl, 5 mM KCl, 0.05 mM EGTA, 1 mM $MgCl_2$, and 6 nM Oregon Green (pH 7.4) at 22°C.

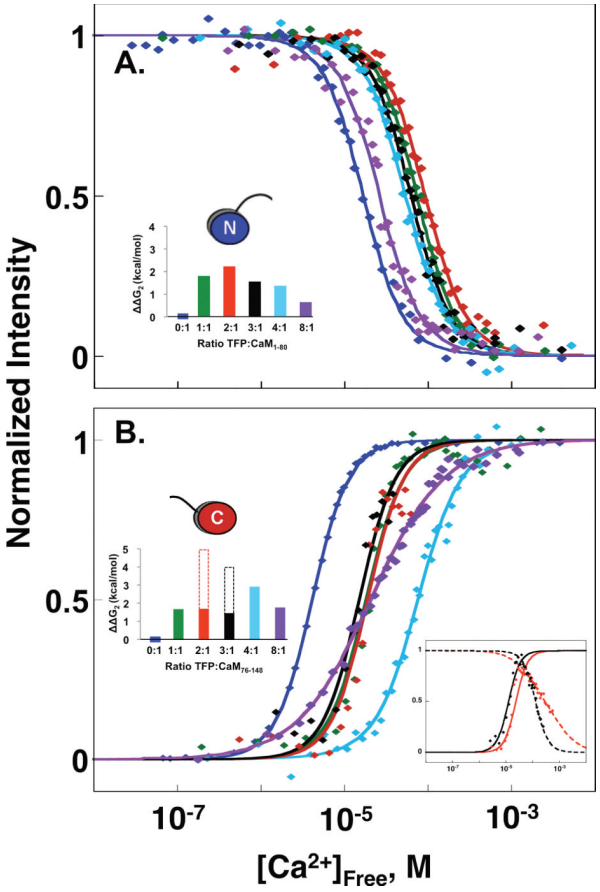

Figure 6. Effect of TFP on Calcium Binding to CaM_{1-80} and CaM_{76-148}

Equilibrium calcium titrations of CaM (6 μM) were conducted in the presence of 0 (blue), 6 (green, 1:1), 12 (red, 2:1), 18 (black, 3:1), 24 (cyan, 4:1), or 48 μM (purple, 8:1 TFP:CaM) TFP, and were monitored using the intrinsic fluorescence of CaM.

A: phenylalanine fluorescence (250 nm_{ex} and 280 nm_{em}).

B: tyrosine fluorescence (277 nm_{ex} and 320 nm_{em}).

In B, for 2:1 and 3:1 TFP:CaM, only the first transition is show. In B, for 4:1 and 8:1 TFP:CaM, the raw signal decreased; it is shown inverted to facilitate comparisons.

Solid curves were simulated according to Eq. 3 and free energies in Table 1; bar graph insets represent $\Delta\Delta G_2$ values in Table 1. Inset in Figure 6B are calcium titration of CaM_{76-148} at 12 μM (red, 2:1 TFP:CaM) and 18 μM (black, 3:1 TFP:CaM) monitored using the intrinsic tyrosine fluorescence of CaM (277 nm_{ex} and 320 nm_{em}). Evidence for multiple species, and piecewise analysis described in *Results*. Solid curves for calcium-dependent increase in fluorescent intensity were simulated according to Eq. 3 and free energies in Table 1; dashed curves correspond to decrease in fluorescence intensity.Solution conditions were 50 mM HEPES, 100 mM KCl, 5 mM KCl, 0.05 mM EGTA, 1 mM $MgCl_2$, and 6 nM Oregon Green (pH 7.4) at 22°C.

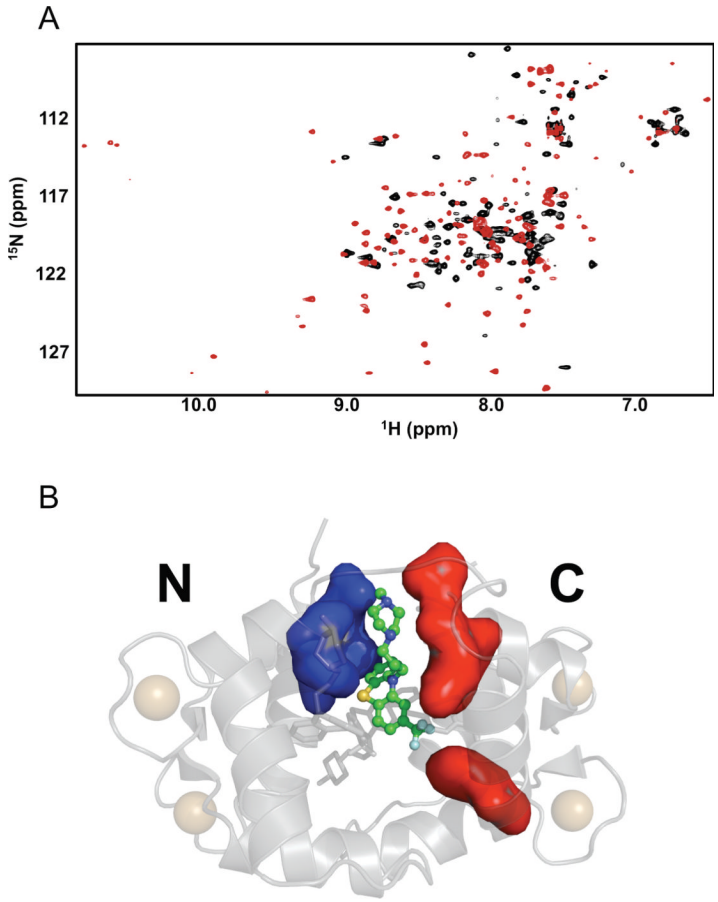

Figure 7. TFP-saturated apo and $(Ca^{2+})_4$-CaM_{1-148}

A. Overlay of ^{15}N-HSQC spectra of apo CaM (black, 2 TFP:CaM) and $(Ca^{2+})_4$-CaM (red, 4 TFP:CaM). Few peaks overlay, indicating significantly different chemical environments for backbone amides in the structures of apo and $(Ca^{2+})_4$-CaM saturated by TFP.

B. Interdomain interactions in $(Ca^{2+})_4$-CaM_{1-148} mediated by TFP. Based on the crystal structure with 4:1 TFP:$(Ca^{2+})_4$-CaM (1LIN.pdb), the TFP molecule shown in ball-and-stick (brown, with fluorine, sulphur, and nitrogen atoms in green, yellow, and blue respectively) interacts with residues in both the calcium-saturated N-domain (blue) and C-domain (red). Those within 4 Å were residues 8, 11, 72, 92, 144, 145, TFP 1, and TFP 2. $(Ca^{2+})_4$-CaM backbone (gray), 4 calcium ions (yellow spheres), and three other TFP (gray sticks) are shown. Figure created with Pymol™.

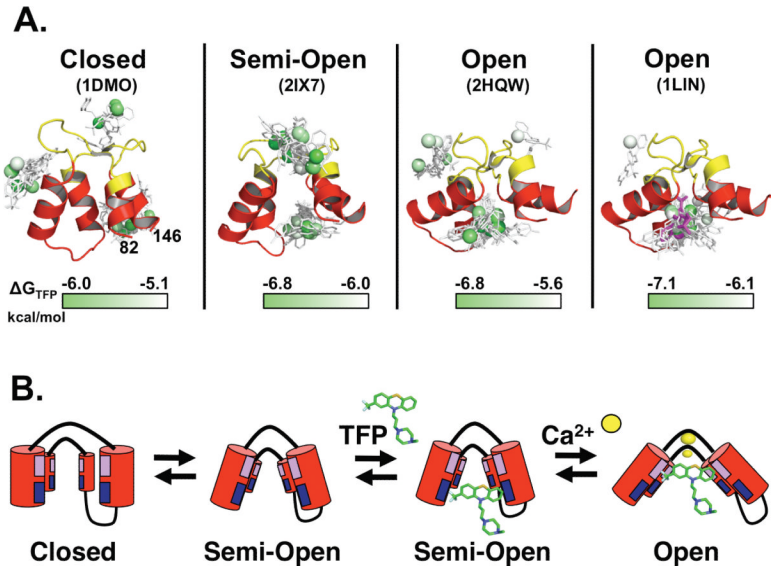

Figure 8. Docking and Models of TFP binding to CaM C-domain

A. TFP Docking to alternative tertiary conformations of apo CaM. Ribbon diagrams of C-domain fragments (residues 82 to 146) represent the “closed” (1DMO.pdb), “semi-open” (2IX7.pdb) and “open” (2HQW, 1LIN.pdb) conformations. Calcium was removed from 2HQW and 1LIN. *AutoDock Vina 1.0.3* [42] predicted positions of TFP binding; 20 models having lowest free energy are shown as sticks. The single sulfur atom of each TFP is shown as a sphere; green corresponds to the most favorable free energy of binding; white is the least favorable. Color thermometer below each set of models indicates the range of energies predicted. The TFP molecule observed at site A of 1LIN.pdb is shown in magenta. Residues in calcium-binding sites are yellow; arrows are included only to orient the viewer to chain direction.

B. Model of conformational transition of apo C-domain in equilibrium between a “closed” and “semi-open” conformation. Binding of TFP to the blue patches accessible in the “semi-open” conformation is energetically more favorable than binding to “closed” form. TFP binding to the blue occludes hydrophobic patches show in purple of the apo C-domain that are otherwise exposed to solvent. An “open” conformation is adopted upon calcium binding, whether alone or also bound to a drug or protein target exposing hydrophobic patches shown in purple.

Table 1

TFP Effects on Calcium Binding to CaM.

		Sites I and II of CaM_{1-148}		Sites III and IV of CaM_{1-148}	
[TFP]	**Ratio**	**ΔG_2[a]**	**$\Delta\Delta G_2$[b]**	**ΔG_2[a]**	**$\Delta\Delta G_2$[b]**
-		-13.05 ± 0.06	-	-15.00 ± 0.06	-
6 μM	1:1	-10.97 ± 0.11	2.08	-12.39 ± 0.07	2.61
12 μM	2:1	-11.57 ± 0.11	1.48	-12.76 ± 0.18	2.24
18 μM	3:1	-11.60 ± 0.16	1.45	-13.23 ± 0.20	1.77
24 μM	4:1	-12.47 ± 0.04	0.58	-13.07 ± 0.09	1.83
48 μM	8:1	-13.59 ± 0.08	-0.54	-13.99 ± 0.06	0.99

		Sites I and II of CaM_{1-80}		Sites III and IV of CaM_{76-148}	
[TFP]	**Ratio**	**ΔG_2[a]**	**$\Delta\Delta G_2$[b]**	**ΔG_2[a]**	**$\Delta\Delta G_2$[b]**
-		-12.91 ± 0.09	-	-14.47 ± 0.12	-
6 μM	1:1	-11.12 ± 0.03	1.79	-12.80 ± 0.08	1.67
12 μM	2:1	-10.70 ± 0.17	2.21	-12.78 ± 0.20[c]	1.69
				-9.55 ± 0.31[d]	4.92
18 μM	3:1	-11.37 ± 0.05	1.54	-13.02 ± 0.18[c]	1.45
				-10.65 ± 0.27[d]	3.82
24 μM	4:1	-11.56 ± 0.05	1.35	-11.56 ± 0.05	2.91
48 μM	8:1	-12.28 ± 0.18	0.63	-12.71 ± 0.21	1.76

[a] **ΔG_2** (kcal/mol) represents apparent total free energy at each indicated ratio of $[TFP]_{total}/[CaM]_{total}$

[b] $\Delta\Delta G_2 = \Delta G_2^{app}$(TFP Added) - ΔG_2 (TFP Absent)

[c] Values determined from initial phase of increasing flourescent signal.

[d] Values determined from decreasing fluorescent signal at higher [calcium].